Journal of Aerosol Science 175 (2024) 106281

Contents lists available at ScienceDirect

Journal of Aerosol Science

journal homepage: www.elsevier.com/locate/jaerosci

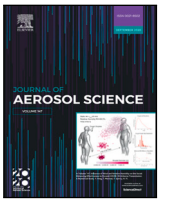

Axisymmetric inertialess model for the capture of airborne microparticles using an electrospray

I.G. Loscertales [a,*], J. Rivero-Rodríguez [a], F.J. Higuera [b], A.J. Hijano [a]

[a] Escuela de Ingenierías Industriales, Universidad de Málaga, Dr. Ortiz Ramos s/n, 29071 Málaga, Spain
[b] ETSIAE, Universidad Politécnica de Madrid, Plaza Cardenal Cisneros 3, 28040 Madrid, Spain

ARTICLE INFO

Editor: Dr. Chris Hogan

Keywords:
Electrosprays
Charged droplet–particle interaction
Particle removal
Filtration
CFD

ABSTRACT

We theoretically analyze the effectiveness of an electrospray of ultrafine droplets to filter out micron sized particles from a gas stream. To that end, we introduce an axisymmetric configuration where the airborne particles merge with the electrospray. The droplets attach to the particles, charging them, and both droplets and charged particles are eventually driven towards a collector by means of an electric field. The attachment process is described through a set of reaction constants based on calculated collision cross-sections, yielding particles with different charge levels. The problem involves computation of the concentrations of each type of particle, the gas flow, and the electric field due to the applied voltages and the space charge. Preliminary numerical simulations show a filtration efficiency that is above 95% for particles larger than about 2 μm and rapidly declines for smaller particles, though this drop of the efficiency can be postponed to smaller particle sizes by decreasing the ratio of particle to electrospray fluxes or the ratio of the inlet velocity of the particle carrying gas to the velocity induced by electric forces inside the device. Pending an exhaustive numerical exploration of the parameter space of the system, these results also show that the gas flow structure, which is strongly affected by the charged particles, is key for high filtration efficiency.

1. Introduction

The capture of airborne particles constitutes the core process of filtration technology. Some times the objective is merely being sure that such particles are withdrawn from a gas stream, regardless of their origin or composition. However, in other applications the objective is precisely the knowledge of their origin or composition. An example is the testing of air quality, where it is essential to determine the composition of the airborne particles, among other things. The basic filtering mechanisms are diffusion, interception, inertial impaction, gravitational settling, electrostatic attraction, diffusiophoresis, thermophoresis and other phoretic mechanisms (Dunnett, 2013). The efficiency of filtering systems relying on the inertia of the particles generally decays for submicrometric particles, while diffusion comes into play only for much smaller particles. There is thus a range of particle sizes, typically between 0.1 μm and 1 μm, where the efficiency of particle removal is low owing to the difficulty of establishing a significant relative velocity between the particles and the carrying gas. Electric forces acting on charged particles offer a means of bridging this gap. Pilat (1975) and Lear, Krieve, and Cohen (1975) investigated the use of electrically charged droplets to collect aerosol particles in a wet scrubber. They reported overall collection efficiencies of 93.6% and 70%, respectively, for particles of about 0.3 μm. Electrostatic precipitators (ESPs) and wet electrostatic precipitators (WESPs) most commonly use a corona discharge (Stommel & Riebel, 2005) to produce ions which, owing to their high diffusivity, are easily attached by the particles and other air contaminants.

* Corresponding author.
E-mail address: loscertales@uma.es (I.G. Loscertales).

https://doi.org/10.1016/j.jaerosci.2023.106281
Received 20 May 2023; Received in revised form 2 October 2023; Accepted 4 October 2023
Available online 6 October 2023

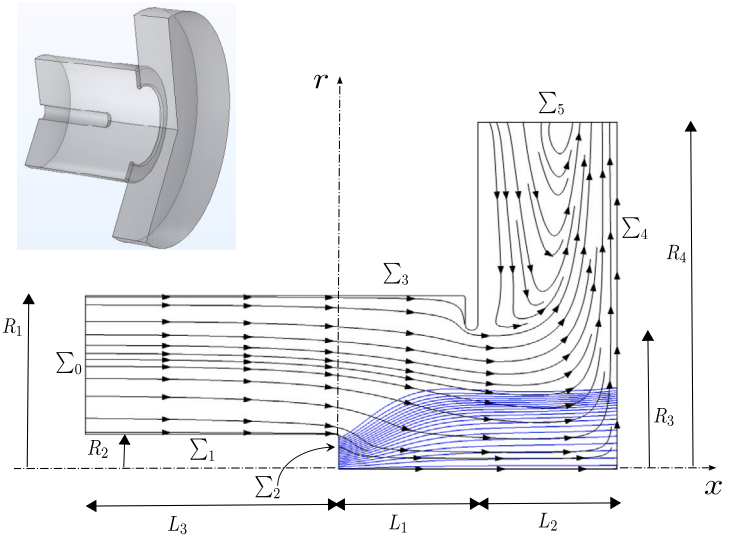

Fig. 1. Sketch of the model setup. Blue lines: electrospray droplets trajectories. Black lines with arrows: gas streamlines. Σ_0 aerosol inlet, Σ_1 inner tube, Σ_2 electrospray inlet, Σ_3 extractor electrode, Σ_4 collector, Σ_5 device exit. Inset: 3D scheme of the device. (For interpretation of the references to color in this figure legend, the reader is referred to the web version of this article.)

The charged particles are then removed by the application of an electric field. Quiet operation and low maintenance are probably the characteristics of ESPs that have led to their extensive use. The relatively high power necessary to generate the corona and the production of ozone as a byproduct of the ionization process are their main drawbacks. Electrosprays offer an alternative to corona discharges to charge aerosol particles. Operating in the cone-jet mode, an electrospray produces a cloud of ultrafine droplets charged to nearly their Rayleigh limit. While the diffusivity of these droplets is small, direct Coulomb and dipolar electric forces suffice for them to act as efficient particle chargers. Fenn (2004) proposed the use of an electrospray to filter out polar or polarizable molecules that might be present in an air stream and could represent an hazard for breathability. Ahn, Yoon, Kim, and Ahn (2003) and Kim, Lee, Kim, and Ogata (2010) compared corona discharges and electrospray droplets as particle chargers for ESPs, and reported a somewhat higher charging efficiency for the latter. In their experiments, large droplets were produced by operating the electrospray in a dripping mode, and the possibility of some corona ions generated along with the electrospray droplets was not excluded. Based on Fenn's idea, the group of Tepper Tepper and Kessick (2008), Tepper, Kessick, and Pestov (2007) developed a device to purify air based entirely on electrosprays, thus avoiding ozone production. Perhaps the first application to our knowledge to use electrospray to collect particles is that of Dziekan (2012), who reported the use of electrosprays to collect lunar dust. He found that the energy required by using an electrospray is only a fraction of that required by other standard filtration methods when working at low pressures. Much more recently, the group of Bango Bango et al. (2021), sparked by the COVID-19 pandemia, demonstrated the use of electrosprays to very efficiently collect airborne bacterias, viruses, spores or prions, for fast monitoring air quality.

The present theoretical work inquires on the basic mechanisms by which electrospray droplets charge airborne particles, and on how such particles are filtered out. To that end, we introduce an axisymmetric design in which ultrafine electrospray droplets mix with a micron sized monodisperse aerosol to promote charging and collection of the latter. The structure of the paper is as follows. Section 2 introduces de mathematical equations that govern the problem. In Section 3 we develop a model for the collision cross section between electrospray droplets and aerosol particles. Section 4 shows the numerical results and the discussion. Finally, Section 5 collects some conclusions.

2. Formulation of the problem

Fig. 1 is a sketch of a device intended to electrically charge and collect airborne microparticles using an electrospray of ultrafine droplets.

The microparticles to be charged are monodisperse, with mass m_p, diameter d_p and very high electrical conductivity, and they are carried by an air stream in the outer tube of a set of two coaxial tubes of radii R_1 and $R_2 < R_1$ (at the left side of the figure). A stream of clean air flows through the inner tube that serves as a sheath to an electrospray source located slightly upstream of the end of this tube. The source generates Φ_e droplets of mass m_e and diameter d_e per unit time, each carrying an electric charge q_e. In what follows, $d_e \ll d_p$ is assumed. Except for the sheath, the electrospray plume and the microparticles are in contact downstream of the inner tube. The outer tube extends to an extractor electrode at a distance L_1 downstream of the inner tube. This electrode is a disk perpendicular to the tube with an orifice of radius $R_3 < R_1$ coaxial with it. A collector electrode, which is a disk of radius $R_4 > R_1$, is set parallel to the extractor at a distance L_2 from it. The inlet of the particle-laden gas is located at a distance L_3 upstream of the inner tube end.

The following notation will be used for the surfaces bounding the system: Σ_0 is the inlet of the microparticles-loaded gas, Σ_1 is the wall of the inner tube, Σ_2 is the inlet of the electrospray plume, Σ_3 is the wall of the outer tube and the extractor, Σ_4 is the collector electrode, and Σ_5 is the outlet of the gas. The distance along the symmetry axis measured from the end of the inner tube is x, and the distance to the axis r.

The extractor electrode and the wall of the outer tube are grounded. The electric potential of the electrospray source and the wall of the inner tube is V_0, and the electric potential of the collector electrode is $-V_1$. The potential is assumed to vary logarithmically between V_0 and 0 at the gas inlet Σ_0, and linearly between 0 and $-V_1$ at the gas outlet Σ_5.

The gas velocity at Σ_0 is assumed to have the Poiseuille distribution for the flow between coaxial cylinders with a flow rate $\pi(R_1^2-R_2^2)v_{g_I}$, which is denoted $v_{g_I} f_p(r/R_1; R_2/R_1)$. The number concentration of microparticles at Σ_0 is uniform at a value n_{0_I}, so, leaving out diffusion around Σ_0, the number of particles that enter the device per unit time is $\Phi_0 = 2\pi n_{0_I} v_{g_I} \int_{R_2}^{R_1} f_p(r/R_1; R_2/R_1) r\,\mathrm{d}r$, which has a given value. The velocity of the sheath gas in the inner tube is $2v_{sh}(1-r^2/R_2^2)$. The carrying gas and the microparticles that are not charged and captured by the collector leave the device moving radially out at Σ_5.

As the microparticles and the electrospray droplets meet, the latter attach to the former, charging them up to a certain level. Since that moment, the already charged particles are dragged by the electric field toward the collector electrode, where they are captured. The state of charge of a particle increases as it grabs droplets, until the electrical repulsion prevents any further droplets from attaching the particle. Thus, aside from the electrospray droplets, a number $N+1$ of different types of particles, with charges from 0 to Nq_e and N to be found, are present in the device. The Stokes numbers $\mathrm{St}_e = (m_e v_c/t_r)/(q_e E_c)$ and $\mathrm{St}_p = (m_p v_c/t_r)/(q_e E_c)$ are assumed to be small, so the effects of the inertia of the droplets and the particles in their transit across the device are negligible. Here v_c and E_c are a characteristic velocity and a characteristic electric field, which are defined in (13) below; $t_r = L_1/v_c$ is a residence time; and it is advanced that the electric force $q_e E_c$ and the drag of the gas are the relevant forces acting on droplets and particles.

2.1. Governing equations

Inertialess electrospray droplets and particles are dragged by the local electric field (charged entities), $\boldsymbol{E}$, and the gas velocity, $\boldsymbol{v}_g$. The continuity equations for droplets and particles are the only ones needed to describe the evolution of each type of entity. In stationary conditions, these equations read

$$\boldsymbol{\nabla}\cdot\left[n_e\left(z_e\boldsymbol{E}+\boldsymbol{v}_g\right)-D_e\boldsymbol{\nabla}n_e\right]=w_e \tag{1}$$

for the electrospray droplets, where n_e is the droplet number concentration, and z_e and D_e are their electrical mobility and diffusivity, respectively. The sink on the right-hand side (for $w_e<0$, as we shall see) accounts for attachment of droplets to the particles. The mobility of the droplets is $z_e = q_e C_e/(3\pi\mu_g d_e)$, where C_e is the Cunningham correction factor of Stokes law for the droplets and μ_g is the viscosity of the gas.

Similarly, for each type of particle,

$$\boldsymbol{\nabla}\cdot\left[n_i\left(z_i\boldsymbol{E}+\boldsymbol{v}_g\right)-D_p\boldsymbol{\nabla}n_i\right]=w_i,\quad i=0,1,\dots N, \tag{2}$$

where n_i and z_i are the number density and the mobility of particles of type i, w_i is the rate of generation of these particles (number of particles of type i generated per unit volume per unit time) due to the *reactions* between droplets and particles of different types, and D_p is the diffusivity of all the particles. The mobility of the particle of type i is $z_i = iq_e C_p/(3\pi\mu_g d_p)$, where C_p is the Cunningham factor for particles.

The Peclet numbers $\mathrm{Pe}_e = v_c L_1/D_e$ and $\mathrm{Pe}_p = v_c L_1/D_p$, with v_c given by (13) below, are large in the conditions of interest, so the effects of diffusion are expected to be small except in thin diffusion layers. Diffusion of droplets and particles could be left out, and the boundary conditions of the following subsection could be simplified accordingly. However, diffusion is retained in the formulation because some artificial diffusivity is required by our numerical treatment. It has been checked by numerical tests that this numerical artifact does nor significantly affect the results.

The problem is closed with a Poisson equation for the electric potential, and mass and momentum conservation equations for the stationary flow of a gas with density ρ_g and viscosity μ_g,

$$\nabla^2\phi=-\frac{1}{\epsilon_0}\left(q_e n_e+\sum_{i=1}^{N}q_i n_i\right),\quad \boldsymbol{E}=-\boldsymbol{\nabla}\phi, \tag{3}$$

$$\boldsymbol{\nabla}\cdot\boldsymbol{v}_g=0, \tag{4}$$

$$\rho_g\boldsymbol{v}_g\cdot\boldsymbol{\nabla}\boldsymbol{v}_g=-\boldsymbol{\nabla}p+\boldsymbol{\nabla}\cdot\tau'+\left(n_e\,q_e+\sum_{i=1}^{N}n_i\,q_i\right)\boldsymbol{E}, \tag{5}$$

In (3), q_e is the charge of the electrospray droplets, which is assumed to be the same for all the droplets, and $q_i = i\,q_e$ is the charge of the particles of type i. In the right-hand side of the gas momentum equation (5), $\tau' = \mu_g\left(\boldsymbol{\nabla}\boldsymbol{v}_g+\boldsymbol{\nabla}\boldsymbol{v}_g^T\right)$ is the viscous stress tensor and the last term is the force that the inertialess droplets and charged particles exert on the unit volume of gas; see, e.g., Khalifehei and Higuera (2020) for a similar formulation for a different problem. The number of types of particles, $N+1$, is to be found as part of the solution.

2.2. Boundary conditions

The boundary conditions are written separately for each variable. For the electric potential, these conditions are

$$\phi(\Sigma_1, \Sigma_2) = V_0, \tag{6a}$$

$$\phi(\Sigma_3) = 0, \tag{6b}$$

$$\phi(\Sigma_4) = -V_1, \tag{6c}$$

$$\phi(\Sigma_0) = V_0 \frac{\ln r/R_1}{\ln R_2/R_1}, \tag{6d}$$

$$\phi(\Sigma_5) = -V_1 \frac{x - L_1}{L_2}, \tag{6e}$$

$$\frac{\partial \phi}{\partial r}(x, 0) = 0, \tag{6f}$$

where (6f) is a symmetry condition at the axis.

Let us call u_g and v_g the axial and radial components of the gas velocity, $\boldsymbol{v}_g$. As mentioned before, we assume a Poiseuille velocity profile with mean velocity v_{g_I} (denoted $v_{g_I} f_P(r)$) at the particle inlet, and a parabolic Poiseuille profile with mean velocity v_{sh} at the sheath gas inlet. We use non-slip conditions at the solid walls, stress free conditions at the outlet, and symmetry at the axis. Accordingly, with $\boldsymbol{e}_r$ denoting a unit radial vector,

$$u_g(\Sigma_1, \Sigma_3, \Sigma_4) = v_g(\Sigma_1, \Sigma_3, \Sigma_4) = 0, \tag{7a}$$

$$u_g(\Sigma_0) = v_{g_I} f_P(r), \quad v_g(\Sigma_0) = 0, \tag{7b}$$

$$u_g(\Sigma_2) = 2v_{sh}\left(1 - r^2/R_2^2\right), \quad v_g(\Sigma_2) = 0, \tag{7c}$$

$$\boldsymbol{e}_r \cdot \tau'(\Sigma_5) = 0, \tag{7d}$$

$$v_g(x, 0) = 0. \tag{7e}$$

We arbitrarily fix the droplet distribution at the electrospray inlet with a truncated Gaussian shape with standard deviation b, adjusted to make the number of droplets injected per unit time equal to a given value Φ_e. Sample computations carried out with the Gaussian replaced by a uniform distribution in an angular sector around the tip of the electrospray meniscus giving the same value of Φ_e yield very similar results as far as the droplets do not fly back toward the electrospray source. We make the number density of droplets zero at the electrodes and the gas inlet, and assume that any droplets left at the gas outlet flow out with the gas. At the symmetry axis, no flux through is allowed. Thus,

$$n_e(\Sigma_2) = Ae^{-r^2/b^2} \quad \text{such that} \quad 2\pi \int_0^{R_2} J_{ex}(0, r) r \, \mathrm{d}r = \Phi_e, \tag{8a}$$

$$n_e(\Sigma_0, \Sigma_1, \Sigma_3, \Sigma_4) = 0, \tag{8b}$$

$$\frac{\partial n_e}{\partial r}(\Sigma_5) = 0, \tag{8c}$$

$$J_{er}(x, 0) = 0, \tag{8d}$$

where J_{ex} and J_{er} are the axial and radial component of the droplet's flux $\boldsymbol{J}_e = n_e\left(z_e \boldsymbol{E} + \boldsymbol{v}_g\right) - D_e \boldsymbol{\nabla} n_e$.

Neutral particles are injected by seeding the gas inlet Σ_0 with a uniform particle concentration n_{0_I}. We assume that the neutral particles do not deposit at the solid walls and do not flow out through the electrospray inlet, and impose symmetry at the axis:

$$n_0(\Sigma_0) = n_{0_I} \quad \text{with} \quad 2\pi n_{0_I} v_{g_I} \int_{R_2}^{R_1} f_p(r/R_1; R_2/R_1) r \, \mathrm{d}r = \Phi_0, \tag{9a}$$

$$\boldsymbol{J}_0(\Sigma_1, \Sigma_2, \Sigma_3, \Sigma_4) \cdot \boldsymbol{n} = 0, \tag{9b}$$

$$\frac{\partial n_0}{\partial r}(\Sigma_5) = 0, \tag{9c}$$

$$J_{0r}(x, 0) = 0, \tag{9d}$$

where $\boldsymbol{n}$ is the unit normal to each element of the boundary, $\boldsymbol{J}_0 = n_0 \boldsymbol{v}_g - D_p \boldsymbol{\nabla} n_0$ is the flux of neutral particles, and J_{0r} is its radial component. The diffusion flux at the gas inlet is neglected.

For the charged particles ($i = 1, \ldots N$) we use,

$$n_i(\Sigma_0, \Sigma_1, \Sigma_2, \Sigma_3, \Sigma_4) = 0, \tag{10a}$$

$$\frac{\partial n_i}{\partial r}(\Sigma_5) = 0, \tag{10b}$$

$$J_{ir}(x, 0) = 0, \tag{10c}$$

where J_{ir} the radial component of the flux of type i particles, $\boldsymbol{J}_i = n_i\left(z_i \boldsymbol{E} + \boldsymbol{v}_g\right) - D_p \boldsymbol{\nabla} n_i$.

2.3. Reactions between entities

We shall assume that the *reactions* that take place between the entities are such that one electrospray droplet of diameter d_e attaches to a neutral particle of diameter d_p to form one charged particle that we call particle type 1, and one electrospray droplet attaches to a particle type 1 to form one particle that we call particle type 2, and so on. The number associated to the particle type refers to the number of electrospray droplets attached to the original neutral particle. This description is based on the fact that, for typical electrospray droplet number concentration, of order $n_e \sim 10^{13}$ m^{-3} near Σ_2, the droplet–droplet separation, which is of order $n_e^{-1/3} \sim 10^{-4}$ m, is much larger than the particle diameter for micron sized particles, $d_p \sim 10^{-6}$ m, so the attaching process may be understood similarly to a free-molecule regime where the electrospray droplets play the role of the gas molecules, with the particle *seeing* the electrospray droplets as individual *molecules*, but not as a continuum fluid. However, an important difference is that the motion of the electrospray droplets is deterministic since, as we shall see, their random velocity is much smaller than the one caused by the drag of the gas and the electric field. We also assume that there is no particle–particle interaction: even if the particles had the same concentration as the electrospray, the collision between the different inertialess entities is caused by their relative velocity, which is due to their different electric mobilities. In the case of microparticles and droplets with diameters d_p and $d_e \ll d_p$, one has that the particle–particle relative velocity, due to their electric mobility difference, is much smaller than the electrospray droplet–particle relative velocity, so the particle–particle collision frequency turns out to be much smaller than the droplet–particle collision frequency and, as we shall see, they have almost no time to collide with each other while flying across the device. Therefore, we solely consider the following reactions

$$1drop + 1p_0 \to 1p_1, \quad 1drop + 1p_1 \to 1p_2, \dots, \quad 1drop + 1p_{N-1} \to 1p_N. \tag{11}$$

From the collision process, one may obtain that the rate of interaction between the different types of particles and the electrospray droplets may be expressed as

$$w_e = -\sum_{i=0}^{N-1} K_i n_e n_i, \quad w_0 = -K_0 n_e n_0, \tag{12a}$$

$$w_i = K_{i-1} n_e n_{i-1} - K_i n_e n_i, \quad i = 1, 2, \dots, N-1, \tag{12b}$$

$$w_N = K_{N-1} n_e n_{N-1}, \tag{12c}$$

where the expressions of the different reaction constants K_i are given in Section 3.

2.4. Dimensionless variables

To write the problem in dimensionless form, we scale distances with L_1, charges with the droplet charge q_e, and use the balances $E_c/L_1 = q_e n_c/\epsilon_0$, $\rho_g v_c^2/L_1 = q_e n_c E_c$ and $\Phi_e = n_c v_c L_1^2$ to define scales for the number densities, n_c, the electric field, E_c, and the velocities, v_c,

$$n_c = \frac{\epsilon_0^{1/4} \rho_g^{1/4} \Phi_e^{1/2}}{q_e^{1/2} L_1^{3/2}}, \quad E_c = \frac{\rho_g^{1/4} q_e^{1/2} \Phi_e^{1/2}}{\epsilon_0^{3/4} L_1^{1/2}}, \quad v_c = \frac{q_e^{1/2} \Phi_e^{1/2}}{\epsilon_0^{1/4} \rho_g^{1/4} L_1^{1/2}}. \tag{13}$$

The electric potential is then scaled with $E_c L_1$, the mobilities with $v_c/E_c = \left(\epsilon_0/\rho_g\right)^{1/2}$, and the diffusivities with $v_c L_1$. The rate constants K_0 to K_{N-1} are scaled with $v_c/(n_c L_1)$, and the collision cross-sections to be discussed in Section 3 with $1/(n_c L_1)$.

Notice that E_c and v_c are the orders of the electric field and the gas velocity induced in the device by a number density of particles of order n_c, each carrying a charge of order q_e. And n_c is the order of the number density of droplets at the electrospray inlet, up to a factor of order $(R_2/L_1)^2$. In the conditions of interest, this E_c is expected to be also the order of the electric field due to the voltages applied to the electrodes, and the inlet velocity of the gas is expected to be of order v_c up to geometrical factors.

In terms of these dimensionless variables, which will be denoted with the same symbols used before for their dimensional counterparts, the equations and boundary conditions keep the same form, except that L_1, q_e, Φ_e and ϵ_0 are replaced by unity.

In particular, the Poisson equation (3) and the gas momentum equation (5) become

$$\nabla^2 \phi = -n_e - \sum_{i=1}^{N} i\, n_i. \tag{3'}$$

$$\boldsymbol{v}_g \cdot \boldsymbol{\nabla} \boldsymbol{v}_g = -\boldsymbol{\nabla} p + \frac{1}{\mathrm{Re}} \nabla^2 \boldsymbol{v}_g + \left(n_e + \sum_{i=0}^{N} i\, n_i \right) \boldsymbol{E}, \tag{5'}$$

where the pressure variations are scaled with $\rho_g v_c^2$ and $\mathrm{Re} = \rho_g v_c L_1/\mu_g$.

Using temporarily asterisks to denote dimensional variables, the parameters that appear in the dimensionless form of the problem are actually

$$V_0 = \frac{V_0^*}{E_c L_1^*}, \; V_1 = \frac{V_1^*}{E_c L_1^*}, \; \Phi_0 = \frac{\Phi_0^*}{\Phi_e^*}, \; v_{g_I} = \frac{v_{g_I}^*}{v_c}, \; v_{sh} = \frac{v_{sh}^*}{v_c}, \; \mathrm{Re}, \tag{14}$$

together with the ratios of each of L_2^*, L_3^*, R_1^*, R_2^*, R_3^*, R_4^* and b^* to L_1^*. In terms of these variables, $n_{0_I} = n_{0_I}^*/n_c = \Phi_0/(v_{g_I} R_1^2 S)$ with $S = 2\pi \int_{R_2/R_1}^1 f_p(\eta; R_2/R_1)\eta \, d\eta$, and the dimensionless constant $A = A^*/n_c$ is adjusted to satisfy (8a) in dimensionless form. In addition to these, the solution of the problem depends on the dimensionless parameter $\hat{q}_e = q_e/(\pi\epsilon_0 d_p^2 E_c)$, which appears in the analysis of the charging process in the following section; see Eq. (21).

For reference, the main roles of these dimensionless parameters are summarized here. For a given particle size, the dimensionless voltage V_0 controls the opening of the spray plume and, together with V_1 and the dimensionless velocities v_{g_I} and v_{sh} of the carrier and sheath gas streams, affects the existence and extent of the recirculation region around the upper corner of the extractor displayed by some of the panels of Fig. 9 below, which turns out to play a crucial role at focusing the particles towards the spray plume and thus increasing the charging rate (see Section 4). The parameter Φ_0 is the flux of microparticles scaled with the flux of electrospray droplets. Moderate values of Φ_0 are required for high capture efficiency. The Reynolds number Re is large in the conditions of interest, but it cannot be arbitrarily increased if the gas flow is to remain laminar. Taking into account the relation $E_c/L_1 = q_c n_c/\epsilon_0$, the droplet charge parameter $\hat{q}_e$ is, up to a factor 1/4, the ratio of the mean volume per droplet, $1/n_c$ (with a number density of droplets of order n_c), to the typical volume swept by a particle in its journey across the device, $(\pi/4)d_p^2 L_1$. Together with the local electric field scaled with E_c, the inverse of the droplet charge parameter is a measure of the number of collisions undergone by a typical particle in the device (Section 3). The droplet charge parameter increases when the size of the particles decreases, which explains the decrease of the collision cross-sections and the capture efficiency for small particles found in Section 4. Finally, some of the geometrical parameters, specially L_2/L_1, R_2/R_1 and R_3/R_1, have a strong effect on the flow pattern in the device, and thus on the focusing of the particles towards the spray plume.

3. Charging process

For convenience, in this section we turn back to dimensional variables. Consider first a neutral particle that moves through the electrospray cloud. Since neutral particles move with the gas, the relative velocity of the electrospray droplets to the particle considered is $z_e \boldsymbol{E}$. Calling σ_c the droplet–particle collision cross-section (to be found), the neutral particle would sweep a volume $\sigma_c z_e E$ per unit time in its motion relative to the droplets, with $E = |\boldsymbol{E}|$. Accordingly, the number of droplets the particle collides with per unit time (the collision frequency) is $f_c = \sigma_c z_e E n_e$. Assuming that attachment occurs for every collision, the rates of depletion of droplets (due to this process only) and neutral particles are

$$-w_0 = -w_e = \sigma_c z_e E n_e n_0, \tag{15}$$

where n_0 is the number concentration of neutral particles.

For typical values $z_e \sim 10^{-5}$ m^2 /(V s), $E \sim 10^5$ V/m, $n_e \sim 10^{13}$ m^{-3}, and taking $\sigma_c \sim (\pi/4)(d_p + d_e)^2$ with $d_p = 5 \times 10^{-6}$ m, one has that $f_c \sim 10^3$ Hz, although the value of σ_c is surely different from $(\pi/4)(d_p + d_e)^2$ due to electric and other interactions, as we shall see.

On the other hand, for $d_e \ll d_p$, the mobility of the charged particles is much smaller than that of the electrospray droplets (by a factor of 100 at least in the cases considered in Section 4), so the particle–particle collision frequency, f_{cp} is smaller than f_c by about the same factor; $f_{cp} \sim 10$ Hz in our cases. In the device depicted in Fig. 1, $L_1 \sim 10^{-2}$ m, with a characteristic velocity $v_c \sim 1$ m/s, so the residence time of the particles within the device would be $t_r \sim 10^{-2}$ s. This means that $f_{cp} t_r \sim 10^{-1}$ whereas $f_c t_r \sim 10$, so the probability of particle–particle collision is much smaller than the electrospray droplet–particle collision probability, which justifies considering only electrospray-particle collisions in this work. Nevertheless, particle–particle collision might need to be taken into account for smaller particles or for other values of the geometrical parameters of the device.

As the particle captures electrospray droplets its charge increases. This charging process may go on until the charge on the particle reaches a saturation value, q_{ps}, when the repulsive electric field created by the charged particle prevents any more droplets from attaching to the particle, which also fixes the maximum number of types of particles, N.

In a general case, the rates of generation of droplets and particles of every type are

$$w_e = -\sum_{i=0}^{N-1} \sigma_i (z_e - z_i) E n_e n_i, \quad w_0 = -\sigma_0 (z_e - z_0) E n_e n_0, \tag{16a}$$

$$w_i = \sigma_{i-1}(z_e - z_{i-1}) E n_e n_{i-1} - \sigma_i (z_e - z_i) E n_e n_i, \quad i = 1, \ldots, N-1 \tag{16b}$$

$$w_N = \sigma_{N-1}(z_e - z_{N-1}) E n_e n_{N-1}, \tag{16c}$$

where $(z_e - z_i)E$ is the relative velocity between the droplets and the particles of type i and σ_i and z_i are the cross section and the electrical mobility of such particle type respectively, with $z_0 = 0$ (uncharged particle). This amounts to

$$K_i = \sigma_i (z_e - z_i) E, \quad i = 0, \ldots, N-1. \tag{17}$$

in Eqs. (12).

To close the problem, one needs to compute the collision cross-section of each type of particle, σ_i, and determine the value of N.

3.1. Model of the collision cross-section

To compute the collision cross-sections of the charging process we proceed from the model introduced by Prem and Pilat (1978). In their work, tiny sub-micronic particles attach to large droplets: our case is the opposite, but the idea prevails. In our case we start from Newton's law for a tiny electrospray droplet approaching a conducting particle of type i and use a reference frame moving with the particle. We assume that the particle does not rotate. The electric field obtained from the solution of the Poisson equation (3) with the boundary conditions (6) at the position of the particle will be named $\boldsymbol{E}_\infty$ in this section, and $\boldsymbol{E}_{ext}(\boldsymbol{x})$ will be this electric field modified by the presence of the conducting particle if it was not charged; the first terms on the right-hand sides of Eqs. (23) below, when evaluated at the position of the droplet. The forces acting on the electrospray droplet are those due to the friction with the gas, to the local external electric field $\boldsymbol{E}_{ext}$, to the Coulomb repulsion between the droplet and the particle (when the particle is charged), to the image force of both the droplet towards the particle and vice versa, and to the Brownian pseudo-force. In addition an inertia force due to the acceleration of the reference frame must be included. Writing these forces in the order they are mentioned, the equation of motion for the electrospray droplet is

$$\begin{aligned} m_e\frac{\mathrm{d}\boldsymbol{v}_e}{\mathrm{d}t} =& -c_{fe}\left(\boldsymbol{v}_e + z_i\boldsymbol{E}_\infty\right) + q_e\boldsymbol{E}_{ext} + \frac{q_e q_i}{4\pi\epsilon_0 r_e^2}\boldsymbol{e}_{r_e} \\ &+ \frac{q_e^2 d_p}{8\pi\epsilon_0}\left[\frac{1}{r_e^3} - \frac{r_e}{\left(r_e^2 - d_p^2/4\right)^2}\right]\boldsymbol{e}_{r_e} + \frac{\epsilon_e - 1}{\epsilon_e + 2}\frac{q_i^2 d_e^3}{16\pi\epsilon_0 r_e^5}\boldsymbol{e}_{r_e} \\ &+ \frac{c_{fe}D_e}{d_p}\left(2 + 0.557\,\mathrm{Re}_p^{0.5}\mathrm{Sc}_e^{0.375}\right)\boldsymbol{e}_{r_e} - m_e\frac{\mathrm{d}\boldsymbol{v}_i^{abs}}{\mathrm{d}t}, \end{aligned} \tag{18}$$

where, as before, m_e is the mass of the droplet and d_p and d_e are the diameters of the particle and the droplet. In addition, $c_{fe} = q_e/z_e = 3\pi\mu_g d_e/C_e$ is the droplet's friction coefficient, and ϵ_0 and ϵ_e are the permittivity of vacuum and the dielectric constant of the liquid the droplets are made of. In this equation, $\boldsymbol{v}_e$ is the droplet-to-particle relative velocity, r_e is the distance between the centers of the particle and the droplet, $\boldsymbol{e}_{r_e}$ is a unit vector in the direction of the line joining these centers, $\boldsymbol{E}_{ext}$ is evaluated at the position of the droplet, and $\boldsymbol{v}_i^{abs}$ is the velocity of the particle relative to the inertial frame tied to the electrodes. The approximation of the Brownian pseudo-force worked out by Johnstone and Roberts (1949) and Prem and Pilat (1978) is used. Here $\mathrm{Re}_p = v_e d_p/\nu_g$, with $v_e = |\boldsymbol{v}_e|$, is the Reynolds number of the effective flow of the droplets relative to the particle, which we estimate as $z_e E_c d_p/\nu_g$, and $\mathrm{Sc}_e = \nu_g/D_e$ is a Schmidt number. It is assumed that this diffusion force acts in the radial direction. Notice that the gas moves with velocity $-z_i\boldsymbol{E}_\infty$ relative to the particle considered.

To assess the importance of each term in (18) let us temporarily introduce the dimensionless variables

$$\hat{t} = \frac{t}{t_c}, \quad \hat{r}_e = \frac{r_e}{d_p/2}, \quad \left(\hat{\boldsymbol{v}}_e, \hat{\boldsymbol{v}}_i^{abs}\right) = \frac{\left(\boldsymbol{v}_e, \boldsymbol{v}_i^{abs}\right)}{v_c}, \quad \hat{\boldsymbol{E}}_{ext} = \frac{\boldsymbol{E}_{ext}}{E_c}, \quad z_c = \frac{v_c}{E_c}, \tag{19}$$

where E_c and v_c were defined in Section 2.4, $t_c = d_p/v_c$ is a time scale adapted to the collision process under scrutiny and z_c is a mobility scale. Eq. (18) then becomes, upon eliminating the friction factor c_{fe} in favor of q_e and z_e,

$$\begin{aligned} \frac{m_e v_c^2}{q_e d_p E_c}\frac{\mathrm{d}\boldsymbol{v}_e}{\mathrm{d}\hat{t}} =& -\frac{z_c}{z_e}\left(\hat{\boldsymbol{v}}_e + \frac{z_i}{z_c}\hat{\boldsymbol{E}}_\infty\right) + \hat{\boldsymbol{E}}_{ext} + \frac{q_i}{\pi\epsilon_0 E_c d_p^2}\frac{1}{\hat{r}_e^2}\boldsymbol{e}_{r_e} \\ &+ \frac{q_e}{\pi\epsilon_0 E_c d_p^2}\left[\frac{1}{\hat{r}_e^3} - \frac{\hat{r}_e}{\left(\hat{r}_e^2 - 1\right)^2}\right]\boldsymbol{e}_r + \frac{\epsilon_e - 1}{\epsilon_e + 2}\frac{2q_i^2/q_e}{\pi\epsilon_0 E_c d_p^2}\left(\frac{d_e}{d_p}\right)^3\frac{1}{\hat{r}_e^5}\boldsymbol{e}_{r_e} \\ &+ \frac{D_e}{d_p z_e E_c}\left(2 + 0.557\,\mathrm{Re}_p^{0.5}\mathrm{Sc}_e^{0.375}\right)\boldsymbol{e}_{r_e} - \frac{m_e v_c^2}{q_e d_p E_c}\frac{\mathrm{d}\hat{\boldsymbol{v}}_i^{abs}}{\mathrm{d}\hat{t}} \end{aligned}$$

or

$$\mathrm{St}_e'\frac{\mathrm{d}\hat{\boldsymbol{v}}_e}{\mathrm{d}\hat{t}} = -\left(\frac{z_c}{z_e}\hat{\boldsymbol{v}}_e + \frac{z_i}{z_e}\hat{\boldsymbol{E}}_\infty\right) + \hat{\boldsymbol{F}}_{ele} + \hat{\boldsymbol{F}}_{dif} - \mathrm{St}_e\frac{\mathrm{d}\hat{\boldsymbol{v}}_i^{abs}}{\mathrm{d}\hat{t}} \tag{20}$$

where $\mathrm{St}_e' = m_e v_c^2/(q_e d_p E_c)$ is a droplet Stokes number measuring the importance of inertial effects during a droplet–particle collision. It is larger by a factor L_1/d_p than the Stokes number St_e defined in Section 2, reflecting the disparity of the time scales of the streaming and collision processes, t_r and t_c,

$$\hat{\boldsymbol{F}}_{ele} = \hat{\boldsymbol{E}}_{ext} + \frac{q_e}{\pi\epsilon_0 d_p^2 E_c}\left[\frac{q_i/q_e}{\hat{r}_e^2} + \left(\frac{1}{\hat{r}_e^3} - \frac{\hat{r}_e}{(\hat{r}_e^2 - 1)^2}\right) + 2\frac{\epsilon_e - 1}{\epsilon_e + 2}\left(\frac{q_i}{q_e}\right)^2\left(\frac{d_e}{d_p}\right)^3\frac{1}{\hat{r}_e^5}\right]\boldsymbol{e}_{r_e},$$

and

$$\hat{\boldsymbol{F}}_{dif} = \frac{k_B T}{q_e d_p E_c}\left(2 + 0.557\,Re_p^{0.5}Sc_e^{0.375}\right)\boldsymbol{e}_{r_e}.$$

Here we have used Einstein's relationship $D_e = z_e k_B T/q_e$, with k_B the Boltzmann constant and T the gas/particle temperature.

3.2. Limit $d_e \ll d_p$

As was mentioned before, we consider situations in which the electrospray droplets are small compared with the particles, $d_e \ll d_p$. This brings in important simplifications to (20). First, the force due to the image of the particle in the droplet (the last term of $\hat{\boldsymbol{F}}_{ele}$) is small compared with the force due to the image of the droplet in the particle (the last-but-one term of $\hat{\boldsymbol{F}}_{ele}$) because of the factor $(d_e/d_p)^3$. Introducing the dimensionless droplet charge

$$\hat{q}_e = \frac{q_e}{\pi\epsilon_0 d_p^2 E_c}, \tag{21}$$

and noticing that $q_i/q_e = i = 0, \dots N$ (because the electric charge acquired by a particle is due to the landing of electrospray droplets on it), the electric force reduces to

$$\hat{\boldsymbol{F}}_{ele} = \hat{\boldsymbol{E}}_{ext} + \hat{q}_e \left[\frac{i}{\hat{r}_e^2} + \left(\frac{1}{\hat{r}_e^3} - \frac{\hat{r}_e}{(\hat{r}_e^2-1)^2} \right) \right] \boldsymbol{e}_{r_e}.$$

We note that, in these conditions, the disparity of sizes translates into a disparity of mobilities, $z_i \ll z_e$: the velocities of the particles relative to the gas are small compared with the velocities of the droplets relative to the gas, and the term $(z_i/z_e)\hat{\boldsymbol{E}}_\infty$ can be neglected in (20). Also, since the velocity of the gas in the device sketched in Fig. 1 is not much larger than the velocity of the particles, $v_i^{abs} \ll v_e$ and the inertia force (the last term of (20)) is small compared with the left-hand side of this equation.

Let us assume that q_e is half of the droplet's Rayleigh limit, $q_e = \sqrt{8\pi^2\gamma\epsilon_0 d_e^3}$. The first factor of the Brownian pseudo-force is then

$$\frac{k_B T}{\left(2\pi^2\gamma\epsilon_0 d_e^3\right)^{1/2} d_p E_c}.$$

Let us consider a situation in which an electrospray of a highly conducting solution is to be used. For instance, highly conducting formamide ($\gamma = 5.84\times10^{-2}$ kg/s, $\epsilon_e = 111$, liquid density $\rho_\ell = 1.130$ kg/m^3) with electrical conductivity $\kappa_\ell = 0.24$ S/m electrosprayed in air. For a liquid flow rate Q_e of the order of the minimum of the cone-jet mode (Fernández de la Mora & Loscertales, 1994), $\rho_\ell Q_e K/(\gamma\epsilon_0\epsilon_e) = 1$, the electric current carried by the spray droplets is $I_e = 9.3\times10^{-8}$ A, the droplet diameter is $d_e = 7.05\times10^{-8}$ m (Loscertales & Fernández de la Mora, 1995), which yields a flux of droplets $\Phi_e = 1.15\times10^9$ s^{-1} and a charge per droplet $q_e = 8.08\times10^{-17}$ C (67% of Rayleigh limit charge), being its mobility $z_e = 4.25\times10^{-5}$ m^2/(V s). Taking $L_1 = 2\times10^{-2}$ m, the characteristic parameters are $n_c = 2.4\times10^{12}$ m^{-3}, $v_c = 1.19$ m/s, $E_c = 4.4\times10^5$ V/m and $z_c = 2.72\times10^{-6}$ m^2/(V s). For a particle with diameter $d_p = 3$ μm, the factor of the Brownian pseudo-force equals 3.8×10^{-5}. On the other hand, one has that

$$\mathrm{Re}_p \sim \frac{z_e E_c d_p}{\nu_g} = \frac{q_e E_c d_p}{c_{fe}\nu_g} = \frac{C_e E_c (2\gamma\epsilon_0)^{1/2} d_e^{3/2}}{3\nu_g\mu_g}\frac{d_p}{d_e} \quad \text{and} \quad \mathrm{Sc}_e = \frac{q_e\nu_g}{z_e k_B T} = \frac{3\pi\nu_g\mu_g d_e}{C_e k_B T},$$

with $\nu_g = \mu_g/\rho_g$, so for 80 nm electrospray droplets in air, and taking $C_e = 1$, one has that $0.557\,\mathrm{Re}_p^{0.5}\mathrm{Sc}_e^{0.375} \sim 3.6$. In fact, $0.557\,\mathrm{Re}_p^{0.5}\mathrm{Sc}_e^{0.375} = O(1)$ for droplets up to 200 nm. Therefore, then Brownian pseudo-force may also be dropped out of (20).

Finally, the droplet Stokes number St_e' for our 70 nm droplet of formamide turns out to be $\mathrm{St}_e' = 1.69\times10^{-3}$. Even for a droplet with diameter 200 nm, the Stokes number would be of order 10^{-2} and therefore the left-hand side of (20) can be dropped out, and this equation finally becomes

$$\frac{z_c}{z_e}\hat{\boldsymbol{v}}_e = \hat{\boldsymbol{E}}_{ext} + \hat{q}_e \left[\frac{i}{\hat{r}_e^2} + \left(\frac{1}{\hat{r}_e^3} - \frac{\hat{r}_e}{\left(\hat{r}_e^2-1\right)^2} \right) \right] \boldsymbol{e}_{r_e}, \tag{22}$$

In brief, under the hypothesis introduced above, the electrospray droplets evolve inertialess in mechanical equilibrium with the surrounding gas even during the stage of attachment to a particle, with the electric force driving the droplets being due to the external field, to their charge, to that on the particle and to their image charge.

In the approximation of (22), the relative velocity of the droplet to the particle is proportional to the total electric field acting on the droplet, given by the right-hand side of (22) (denoted $\hat{\boldsymbol{E}}$ in what follows). This field follows from the solution of Laplace's equation with a uniform electric field $\boldsymbol{E}_\infty$ far from the particle and two bodies at given positions; one of them (the droplet) being a point charge, and the other (the particle) a charged equipotential sphere. The solution of this problem is written here as the sum of the electric field around an uncharged equipotential particle in the absence of droplet ($\boldsymbol{E}_{ext}$) plus the electric field due to the charge of the equipotential particle redistributed by the presence of the droplet but in the absence of far field (this second contribution is computed using the method of images). Both contributions satisfy the Laplace equation and the condition that the particle is equipotential. The first contribution satisfies, in addition, the condition at infinity. The parameter $\hat{q}_e$ measures the relative importance of the second to the first of these contributions to the electric field.

Let $\hat{x}$ be the distance from the center of the particle in the direction of $\hat{\boldsymbol{E}}_\infty$ and $\hat{y}$ the distance perpendicular to this direction in the plane containing the centers of the particle and the droplet. To compute the collision cross-section it suffices to determine the path of the glancing droplet; i.e., the droplet that just touches the particle coming from $(-\infty, \hat{y}^*)$, and such that droplets coming from $\hat{y} > \hat{y}^*$ at infinity do not reach the particle. To find $\hat{y}^*$ it is convenient to write the right-hand side of (22) in spherical coordinates

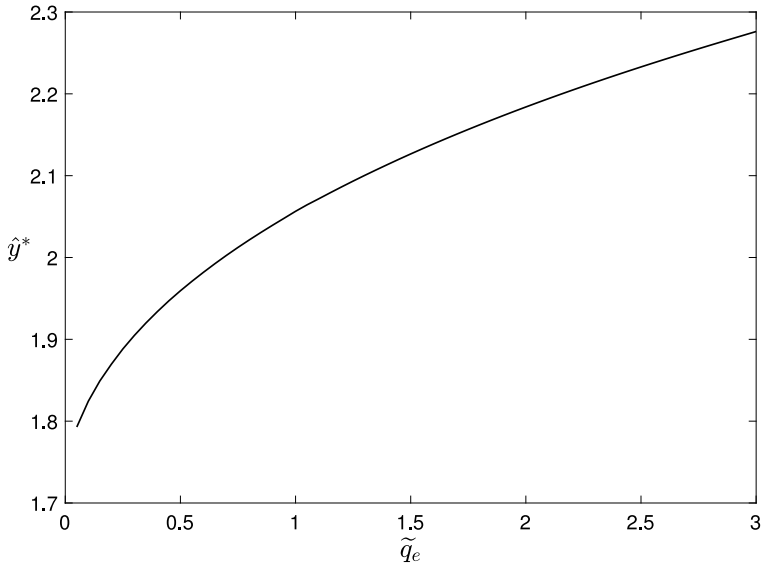

Fig. 2. Values of $\hat{y}^*$ versus $\widetilde{q}_e$ for $i = 0$.

(r_e, θ_e) with origin at the center of the particle and the polar line $\theta_e = 0$ in the direction of $\hat{\boldsymbol{E}}_\infty$,

$$\hat{E}_r = \hat{E}_\infty \left(1 + \frac{2}{\hat{r}_e^3}\right) \cos\theta_e + \frac{i\hat{q}_e}{\hat{r}_e^2} + \hat{q}_e \left[\frac{1}{\hat{r}_e^3} - \frac{\hat{r}_e}{\left(\hat{r}_e^2 - 1\right)^2}\right],$$
$$\hat{E}_\theta = -\hat{E}_\infty \left(1 - \frac{1}{\hat{r}_e^3}\right) \sin\theta_e, \tag{23}$$

where $\hat{E}_\infty = \left|\hat{\boldsymbol{E}}_\infty\right|$ and i is the number of electrospray droplets previously attached to the particle.

The path of a droplet satisfies

$$\hat{r}_e \frac{\mathrm{d}\theta_e}{\mathrm{d}\hat{r}_e} = \frac{\hat{E}_\theta}{\hat{E}_r}. \tag{24}$$

We integrate this equation starting far ahead of the particle, at a certain $\hat{r}_e = \hat{r}_\infty \gg 1$, with various values of θ_e at this far point, say θ_0, and determine $\hat{y}^*$ as the maximum value of $\hat{r}_\infty \sin\theta_0$ for which the path reaches the surface of the droplet. This computation can be done accurately because the paths that reach the surface do so perpendicularly, as $\hat{E}_r \to -\infty$ when $\hat{r}_e \to 1$.[1] The result does not depend on $\hat{r}_\infty$, provided it is large.

Inspection of (23) immediately shows that the right-hand side of (24) depends only on i and $\widetilde{q}_e = \hat{q}_e / \hat{E}_\infty$, so $\hat{y}^* = \hat{y}^*\left(i, \widetilde{q}_e\right)$. In terms of this $\hat{y}^*$, the dimensionless cross-section $\hat{\sigma}_i$ is, in the approximation used,

$$\hat{\sigma}_i = \pi \hat{y}^{*2} \tag{25}$$

or, in dimensional variables,

$$\sigma_i = \frac{\pi d_p^2}{4} \hat{y}^{*2}. \tag{26}$$

Having completed the analysis of the attachment process, we suppress the subscript ∞, which is no longer necessary, from the electric field computed from (3) and (6). We return to the notation $\boldsymbol{E}$ from this point.

Fig. 2 shows the values of $\hat{y}^*$ obtained upon integration of (24) for $i = 0$. In this case the particle is uncharged, so the effect of $\hat{q}_e$ (or $\widetilde{q}_e$) on $\hat{y}^*$ is due to the image charge, which is attractive and increases as $\hat{q}_e$ does, yielding a continuous growth of $\hat{y}^*$.

Fig. 3 shows $\hat{y}^*$ versus $\widetilde{q}_e$ for several values of $i \geq 1$. As can be seen, $\hat{y}^*$ decreases when $\widetilde{q}_e$ increases, due to the growing importance of the repulsion between the already charged particle and the approaching electrospray droplet, reaching $\hat{y}^* = 0$ (in the approximation used) for values of $\widetilde{q}_e$ larger than a certain $\widetilde{q}_{ps}(i)$. For instance, $\widetilde{q}_{ps} \approx 7.51$ for $i = 1$ (rightmost curve in Fig. 3), indicating that the maximum number of electrospray droplets that can attach to the originally neutral particle is just 1 when $\widetilde{q}_e$ is larger than this value or, in other words, the saturation charge for $i = 1$ (scaled with $\pi\epsilon_0 d_p^2 E$) is about 7.51. The behavior is similar for other values of i in Fig. 3, yielding the values of the saturation charge, $\widetilde{q}_{ps}(i)$, given in Table 1.

[1] The expression of the image charge field in (23) ceases to be valid as the droplet approaches the surface of the particle, even when the diameter of the droplet is taken into account.

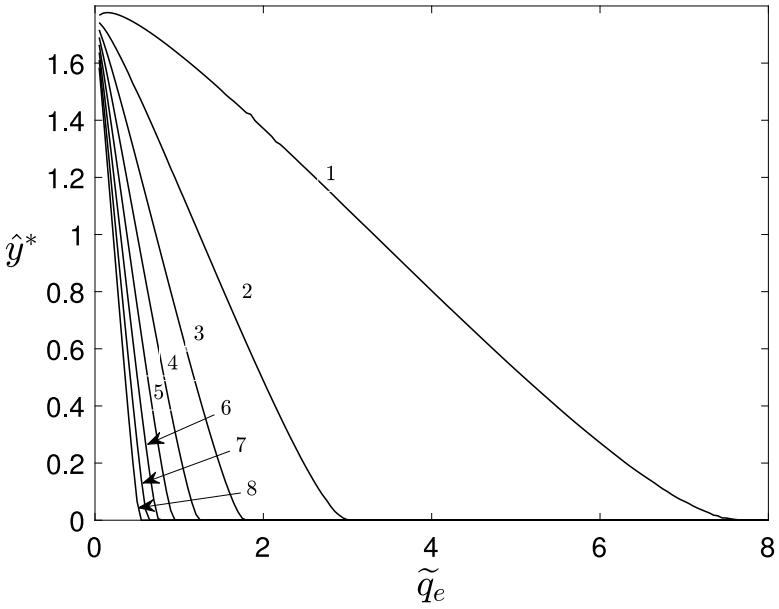

Fig. 3. Values of $\hat{y}^*$ versus $\widetilde{q}_e$ for $i = 1, \ldots 8$. The number on the curve indicates the corresponding value of i.

Table 1
Values of the dimensionless saturation charge, $\widetilde{q}_{ps}$, for different values of i.

i	1	2	3	4	5	6	7	8
$\widetilde{q}_{ps}$	7.51	2.94	1.76	1.22	0.93	0.75	0.63	0.53

This means that, for instance, when $\widetilde{q}_{ps}(5) \le \widetilde{q}_e \le \widetilde{q}_{ps}(4)$ the maximum number of electrospray droplets that can attach to a particle is 5, so one would expect a population of particles with 0, 1, 2, 3, 4 and 5 electrospray droplets attached, in other words, $N = 5$. A similar situation occurs when $\widetilde{q}_{ps}(4) \le \widetilde{q}_e \le \widetilde{q}_{ps}(3)$, with $N = 4$, and so on.

To have an idea of possible values of $\widetilde{q}_e$, let us assume again that the electrospray droplet is charged at half of its Rayleigh limit, which yields

$$\widetilde{q}_e = \frac{q_e}{\pi \epsilon_0 E d_p^2} = \left(\frac{2\gamma d_e^3}{\epsilon_0 E^2 d_p^4} \right)^{1/2}.$$

For a given electrospray, the value of $\widetilde{q}_e$ varies as the inverse of the applied field and with the inverse of the square of the size of the neutral particles, and N varies accordingly. On the other hand, $\widetilde{q}_e$ increases with the droplet size to the power of 3/2, which leads to a decrease of N. For typical values of $\gamma = 10^{-2}$ kg/s^2, $d_p = 10^{-6}$ m, $d_e = 80$ nm and $E = 5 \times 10^4$ V/m, one obtains $\widetilde{q}_e = 21.5$, whereas if $d_p = 5 \times 10^{-6}$ m then $\widetilde{q}_e = 0.86$. In the former case $N = 1$ whereas in the latter $N = 10$ or more. If $d_e = 200$ nm instead, then $\widetilde{q}_e = 85$ for $d_p = 10^{-6}$ m and $\widetilde{q}_e = 3.4$ for $d_p = 5 \times 10^{-6}$ m, which lead to $N = 2$ and $N = 1$, respectively. Therefore, the analysis of the cross-section yields the number of particle types, N, that will appear in the problem.

Note that, for a given experimental setup, electrospray conditions and type of particles, the values of E_c, γ, d_e and d_p are fixed, and so is the value of $\hat{q}_e$. Therefore, it may be convenient to calculate $\hat{y}^*$, for such a fixed value of $\hat{q}_e$. Fig. 4 shows $\hat{y}^*$ versus the dimensionless external electric field strength, $\hat{E}$, for several values of i and a fixed value of $\hat{q}_e = 3.5$. The most interesting feature in Fig. 4 is that, for a given value of $\hat{q}_e$, the value of N depends on $\hat{E}$, so N must be calculated as part of the solution. For values of $\hat{E} \gg \hat{q}_e$, $\hat{y}^*$ should asymptotically go to the value of $\hat{y}^* \left(i \to 0, \widetilde{q}_e \to 0\right) \approx 1.78$ (see Fig. 2) whereas $N \to \infty$.

4. Numerical results

4.1. Base case

Let us consider the following case in which the geometry of the experimental setup is characterized by the dimensionless data given in Table 2, with $L_1 = 2 \times 10^{-2}$ m. The parameter esp stands for the thickness of the extractor.

The characteristics of the neutral particles are listed in Table 3, and the mobilities of the charged particles are in Table 4.

We shall use an electrospray of highly conducting formamide, whose properties and outcome are collected in Table 5 (Loscertales & Fernández de la Mora, 1995). To assess the electrospray flow rate we have resorted to Fernández de la Mora and Loscertales (1994):

$$Q_e = \frac{\gamma \epsilon_0 \epsilon_e}{\rho_\ell \kappa_\ell}.$$

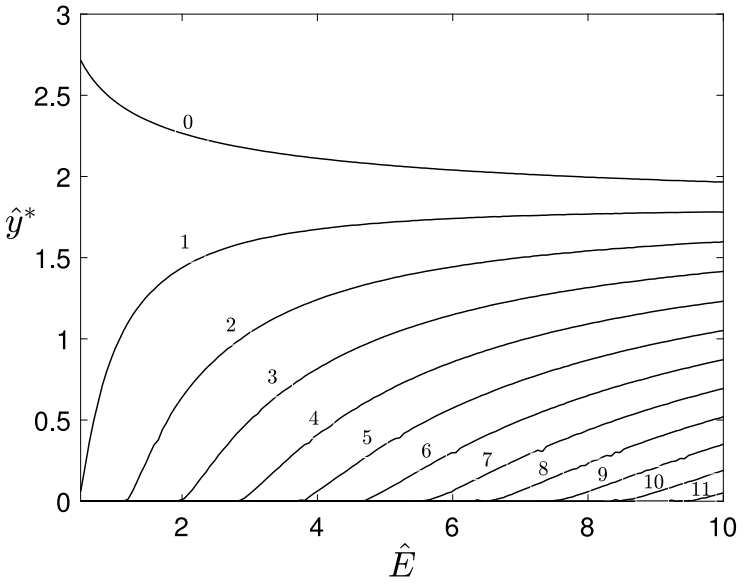

Fig. 4. Values of $\hat{y}^*$ versus $\hat{E}$ for $i = 0, 1, 2, \ldots 11$. In this case $\hat{q}_e = 3.5$. The number on the curve indicates the corresponding value of i.

Table 2
Dimensionless setup geometry. $L_1^* = 2 \times 10^{-2}$ m.

L_2	L_3	R_1	R_2	R_3	R_4	esp
1	2	1.5	0.2	1	3	0.1

Table 3
Characteristics of the neutral particles.

d_p (m)	ρ_p (kg/m^3)	m_p (kg)	c_{fp} (kg/s)
1.37×10^{-6}	10^3	1.35×10^{-15}	1.16×10^{-10}

Table 4
Electrical mobility of the charged particles, m^2/(V s).

z_1	z_2	z_3	z_4	z_5	z_6
6.83×10^{-7}	1.37×10^{-6}	2.05×10^{-6}	2.73×10^{-6}	3.42×10^{-6}	4.10×10^{-6}

Table 5
Characteristics of the electrospray.

κ_ℓ (S/m)	ϵ_e	γ (kg/s^2)	ρ_ℓ (kg/m^3)	Q_e (m^3/s)	I_e (A)
2.4×10^{-1}	111	5.84×10^{-2}	1.13×10^3	2.1×10^{-13}	9.28×10^{-8}
d_e (m)	Φ_e (s^{-1})	q_e (C)	c_{fe} (kg/s)	z_e (m^2/(V s))	m_e (kg)
7.03×10^{-8}	1.16×10^9	8.01×10^{-17}	1.89×10^{-12}	4.24×10^{-5}	2.05×10^{-19}

With these data one has $E_c = 4.41 \times 10^5$ V/m, $v_c = 1.19$ m/s, $n_c = 2.42 \times 10^{12}$ m^{-3} and $z_c = 2.71 \times 10^{-6}$. The charge parameter in (21) turns out to be $\hat{q}_e = 3.5$; thus, according to Fig. 4, for values of E of order one, one would expect particles of types 0 and 1 almost exclusively. For the rest of dimensionless parameters in (14) and the lines following this equation we choose $V_0 = 0.227$, $-V_1 = -0.283$, $\Phi_0 = 8.6 \times 10^{-2}$, $v_{g_I} = v_{sh} = 0.25$, $\mathrm{Re} = 2.87 \times 10^3$ and $b = 0.3 R_2$.

The values of the reaction constants K_i are computed as part of the solution, using the dimensionless cross sections for $\hat{q}_e = 3.5$ (Fig. 4).

For the numerical treatment we use the finite elements software COMSOL Multiphysics® (COMSOL, 2021), writing the problem in its weak form. As was mentioned in Section 2, the values of the real diffusivities in (1) and (2) (not shown) are so small that the diffusion terms could be dropped out from the conservation equations. However, for numerical reasons we have included small artificial diffusivities. We have used the values $D_e = D_p = 10^{-4}$ to compute the stationary state solutions discussed in this section. Values smaller than these have not been tried because they require reducing the size of the mesh elements, which leads to a large increase in the computational time with no variation in the results.

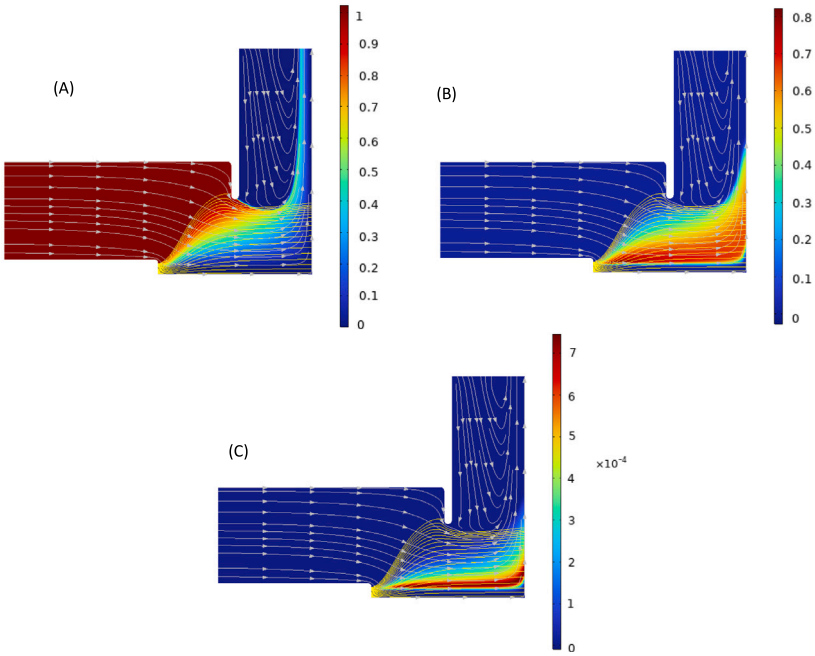

Fig. 5. Particle concentration made dimensionless with the neutral particles input concentration (color code), electrospray flux lines (yellow) and gas streamlines (gray lines with arrows) for type: (A) $i = 0$, (B) $i = 1$ and (C) $i = 2$. Re $= 2.87 \times 10^3$, $\hat{q}_e = 3.15$, $V_0 = 0.227$, $-V_1 = -0.283$, $\Phi_0 = 8.6 \times 10^{-2}$, $v_{g_I} = 0.25$ and $v_{sh} = 0.25$. Red: highest, blue: zero. (For interpretation of the references to color in this figure legend, the reader is referred to the web version of this article.)

Table 6
Filtering efficiency, ef (%), and % contributed by each type of charged particle captured at the collector, Σ_4.

e_f	$e_f(+1)$	$e_f(+2)$
78.14	78.01	0.13

Fig. 5 shows the dimensionless particle concentrations for particles type 0 (neutral ones) 1 and 2 in a section of the device through the symmetry axis. As expected, since the dimensionless field strength is $O(1)$, the concentration of particles of type 2 is about 1000 times smaller than that of particles of type 1, and the concentration of particles type 3 (not shown) is more than 10^{10} times smaller, so in this case essentially $N = 1$. The characteristic droplets and neutral particles dimensionless concentrations at their corresponding inlets turn out to be $A = 25.9$ and $n_{0_I} = 0.176$.

Fig. 6 shows the radial distribution of the dimensionless flux of particles of type 1 reaching the collector, $J_{1x}(2, r)$.

The filtering or capturing efficiency, e_f, is defined as one minus the ratio of the total flux of neutral particles escaping the domain through the gas outlet to the total flux of neutral particles entering the domain,

$$e_f\ (\%) = \left(1 - \frac{\int_{\Sigma_5} \boldsymbol{J}_0 \cdot \boldsymbol{n}\, \mathrm{d}s}{\Phi_0}\right) \times 100 = \left(1 - \frac{J_{05}}{J_{00}}\right) \times 100. \tag{27}$$

In this case, the filtering efficiency is $e_f = 78\%$. Since, according to the boundary conditions, the neutral particles cannot stick to the wall, the filtering is due to the charging efficiency combined with the electric field that drives the charged particles towards the collector disk at the right-hand side of Fig. 1. Table 6 shows the total efficiency e_f and the separate contributions of each type of charged particles that are collected on Σ_4, $100 \times J_{i4}/J_{00}$, for $i = 1, 2$ (denoted $e_f(+i)$).

In this example, the filtering is relatively poor (78%). However, it strongly depends on the operation parameters, especially on the values of v_{g_I} and v_{sh}, as shown in Fig. 7. By simply reducing the values of both velocities down to 0.126 while keeping the rest of the parameters constant, the efficiency increases to 88,6%. In the following sections, for a given electrospray we investigate the role played by the particle diameter and flux, d_p and Φ_0, and by the gas flow rate via v_{g_I}.

4.2. Effect of particle size

We have solved the set of equations for particles' diameters d_p from 1 to 5 μm for the same dimensionless parameters: $V_0 = 0.227$, $-V_1 = -0.283$, $\Phi_0 = 8.6 \times 10^{-2}$, $v_{g_I} = v_{sh} = 0.25$ and Re $= 2.87 \times 10^3$. Therefore, the only parameter that varies is $\hat{q}_e$. Fig. 8 shows

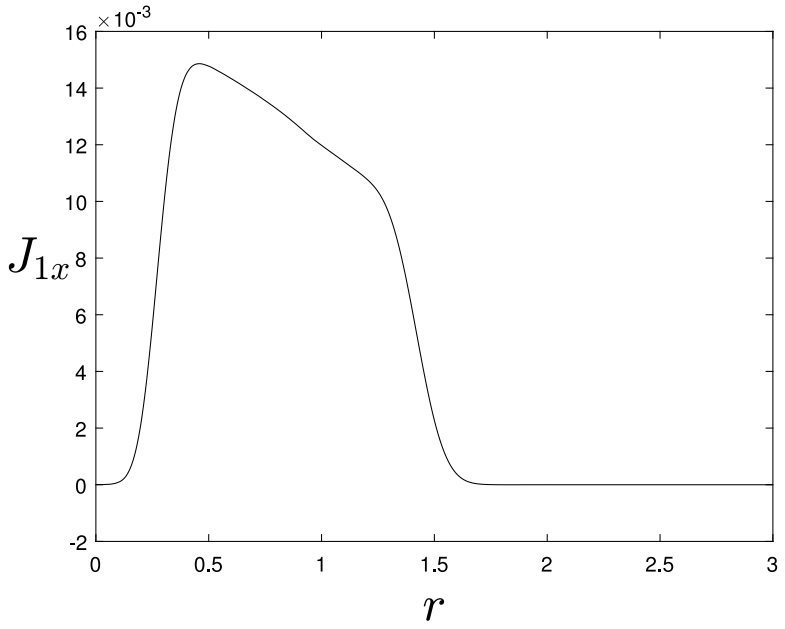

Fig. 6. Flux of the charged particles type 1 on the collector, Σ_4, $J_{1x}(r,2)$, Re $= 2.87\times10^3$, $\hat{q}_e = 3.15$, $V_0 = 0.227$, $-V_1 = -0.283$, $\Phi_0 = 8.6\times10^{-2}$, $v_{g_I} = 0.25$ and $v_{sh} = 0.25$.

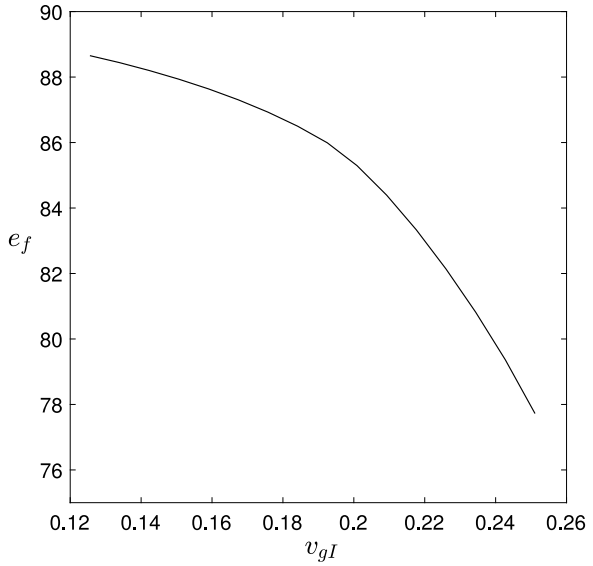

Fig. 7. Filtering efficiency e_f as a function of v_{g_I} for Re $= 2.87\times10^3$, $\hat{q}_e = 3.15$, $V_0 = 0.227$, $-V_1 = -0.283$, $\Phi_0 = 8.6\times10^{-2}$ and $v_{sh} = v_{g_I}$.

Table 7
Percentage of particles captured by type.

d_p	$e_f(+1)$	$e_f(+2)$	$e_f(+3)$	$e_f(+4)$	$e_f(+5)$	$e_f(+6)$
1 μm	56.33	7.5×10^{-2}	0	0	0	0
1.37 μm	77.69	5.2×10^{-2}	0	0	0	0
2 μm	92.70	2.51	0	0	0	0
3 μm	53.05	45.09	1.16	0	0	0
4 μm	17.73	58.37	22.60	1.19	3.2×10^{-3}	0
5 μm	4.16	37.86	43.16	13.39	1.34	1.6×10^{-2}

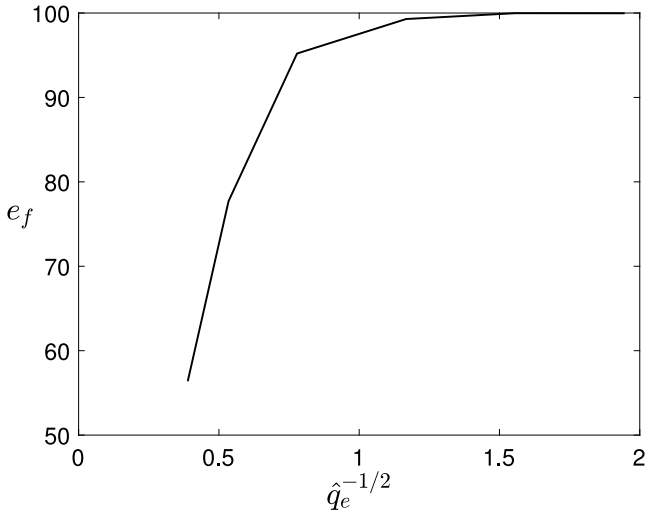

Fig. 8. Filtering efficiency e_f versus $\hat{q}^{-1/2} \propto d_p$. Re $= 2.87 \times 10^3$, $V_0 = 0.227$, $-V_1 = -0.283$, $\Phi_0 = 8.6 \times 10^{-2}$ and $v_{sh} = v_{g_l} = 0.25$.

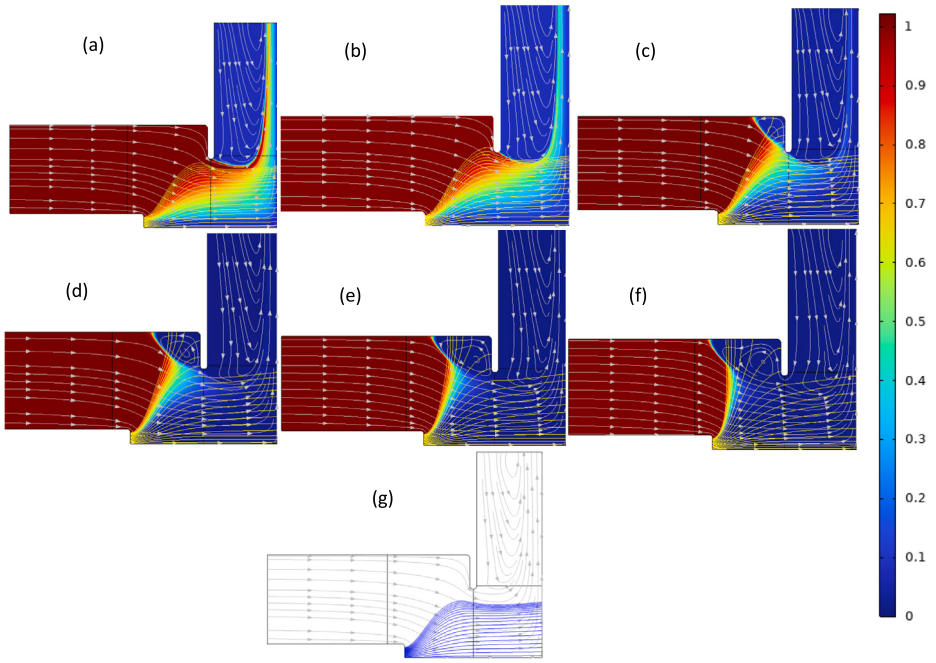

Fig. 9. Neutral particles concentration made dimensionless with its input concentration (color code), electrospray flux lines (yellow) and gas streamlines (gray lines with arrows) for: (a) $d_p = 1$ μm ($\hat{q}_e = 6.61$), (b) $d_p = 1.37$ μm ($\hat{q}_e = 3.5$), (c) $d_p = 2$ μm ($\hat{q}_e = 1.65$), (d) $d_p = 3$ μm ($\hat{q}_e = 0.734$), (e) $d_p = 4$ μm ($\hat{q}_e = 0.431$) and (f) $d_p = 5$ μm ($\hat{q}_e = 0.246$). Re $= 2.87 \times 10^3$, $V_0 = 0.227$, $-V_1 = -0.283$, $\Phi_0 = 8.6 \times 10^{-2}$ and $v_{sh} = v_{g_l} = 0.25$. (g) gas flow pattern and electrospray flux lines when no particles are injected. (For interpretation of the references to color in this figure legend, the reader is referred to the web version of this article.)

the capture efficiency, e_f versus $\hat{q}_e^{-1/2}$, which is proportional to d_p. For these conditions, the efficiency dramatically decreases for particles smaller than 2 μm (i.e. $\hat{q}_e^{-1/2} < 0.779$).

Table 7 shows the filtering efficiency for each particle size split according to the particle type that are collected. As expected, as d_p increases (or $\hat{q}_e$ decreases) the maximum particle type, N, increases, reaching 6 for $d_p = 5$ μm in this case. It might seem that e_f increases with d_p because N does, but the main reason is the gas flow pattern that develops. Fig. 9 shows the flow patterns for the six cases considered in Table 7. The color code in Fig. 9(a) to (f) is for the concentration of neutral particles (type 0) relative to their inlet concentration. The yellow lines stand for the flux of electrospray droplets and the gray lines are streamlines of the gas. Fig. 9(g) shows the gas streamlines and electrospray flux lines when no particles are injected. In panels (c) to (f) there is a gas recirculation zone around the corner of the extractor and the particle laden gas is focused towards the electrospray plume, which

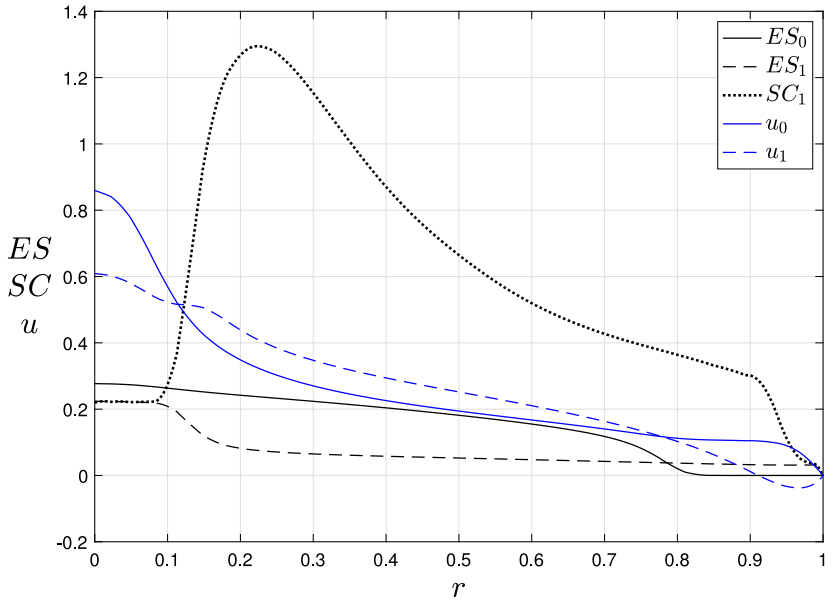

Fig. 10. Electrospray charge concentration, ES, total charge concentration, SC, and axial gas velocity, u, at the extractor plane for cases in Fig. 9(g) (labeled as $_0$) and Fig. 9(f) (labeled as $_1$). (For interpretation of the references to color in this figure legend, the reader is referred to the web version of this article.)

partially reaches the extractor and the outer tube wall. This enhances particle charging, leading to a large flux of charged particles of type 1 and up. The electric force acting on these particles is partially transferred to the gas, which accelerates axially towards the collector provoking a radial suction around the extractor hole and substantially changing the flow pattern (compare with Fig. 9(g)). In addition, since the charged particles are much slower than the electrospray droplets, the volumetric space charge increases in the *reaction* zone, causing the opening of the electrospray plume.

In the cases shown in Fig. 9(a) and (b) the gas flow does not exhibit this recirculation zone. The reason is the rather small cross section σ_i for these cases compared to those for larger particle diameters. This leads to a much lower charging fraction, which in turn leads to a much smaller injection of momentum into the gas stream. As a result, a rather large part of the particle laden gas goes through the extractor across a region where the droplet density is very low, so the collision events between the particles and the droplets seldom occur, resulting in a very low charging efficiency and therefore a very low capture efficiency.

Fig. 10 shows several dimensionless variables at the extractor plane ($x = 1$, $0 \le r \le R_3 = 1$) for cases (f) and (g) in Fig. 9. ES_0 and u_0, continuous black and blue lines, represent respectively the electrospray charge concentration and the gas axial velocity when no particles are injected (case (g) in Fig. 9). The electrospray concentration, space charge concentration and axial gas velocity for the case (f) in Fig. 9 are represented by ES_1, SC_1 and u_1 respectively; in this case SC_1 includes the charge concentration due to the electrospray and to the charged particles. As mentioned before, the density of charged particles leadss to a substantial increase of the space charge compared to that due to the electrospray alone because of their lower electric mobility, causing a widening of the electrospray plume and also injecting axial momentum to the gas, which increases its axial velocity in a region $0.1 < r < 0.8$ approximately. Note the reverse axial flow region that forms close to the edge of the extractor orifice at $r = 1$ to conserve the total gas flow. In this example, a substantial fraction of the electrospray charge is transferred to the particles leading to a high filtering efficiency. It is also noteworthy to mention that, in this configuration, the core of the electrospray, $r < 0.1$ approximately, remains empty of particles, due mainly to the sheath gas injected through the electrospray inlet.

4.3. Low particle concentration

Clearly, the gas flow field is key to the capture efficiency. In this section we shall select the dimensionless parameters such that the particle size (or $\hat{q}_e$) does not significantly affect the gas flow field, while forcing the particle laden stream to pass across the electrospray plume. This is achieved mainly by reducing the particle flux, Φ_0, and reducing also the gas injection velocities v_{g_I} and v_{sh}. In particular, we use the values collected in Table 8. For these small values of v_{g_I} and v_{sh}, the wind induced by the electrospray creates a tiny recirculation zone close to the extractor hole and focuses the particle laden gas towards the axis of the device, forcing it to go across the central part electrospray plume. On the other hand, the value of Φ_0 is chosen such that the momentum injected in the gas stream by the larger particles (5 μm) when charged only causes a small change of the original flow field (i.e. without particles injected). Although for the smaller particles one could increase Φ_0 by a factor of 100 without affecting the gas flow field, we have chosen to keep Φ_0 constant for the sake of comparison.

Table 8
Dimensionless parameters used.

Re	V_0	$-V_1$	Φ_0	v_{sh}	v_{g_l}
2.87×10^3	0.227	−0.283	8.63×10^{-4}	4.2×10^{-2}	8.4×10^{-2}

Table 9
Results for the parameters shown in Table 8.

d_p (μm)	0.5	1	1.37	2	3	4	5
$\hat{q}_e^{-1/2}$	0.195	0.389	0.535	0.779	1.167	1.556	1.946
N	1	2	2	2	3	5	6

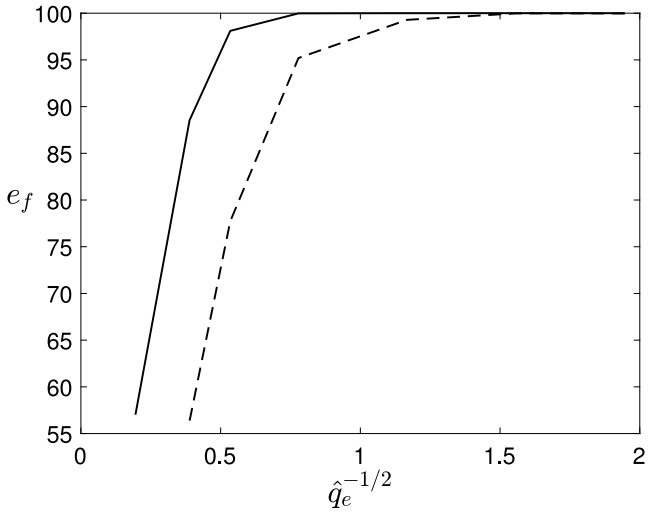

Fig. 11. Efficiency e_f versus $\hat{q}_e^{-1/2}$. Solid line: results for the parameters given in Table 8. Dashed line: results given in Fig. 8 (for comparison).

Table 9 shows the values of $\hat{q}_e^{-1/2}$ and N obtained with the parameters in Table 8 for different particle diameters. The first row shows the diameter of the particles, the second shows the corresponding value of $\hat{q}_e^{-1/2}$ and the third one shows the corresponding value of N. As before, N increases when $\hat{q}_e$ decreases or, equivalently, when d_p increases.

Fig. 11 shows the filtering efficiency, e_f, versus $\hat{q}_e^{-1/2}$. The solid line corresponds to the results with the parameters in Table 8 whereas the dashed line is the result already given in Fig. 8 just for comparison. In this case the gas flow is practically the same for all cases, so the differences in collection efficiency are associated to the particle size. Roughly, the charging collision cross section σ_i varies as d_p^2, so a decrease of the particle diameter strongly reduces the cross sections. Therefore, only the particles that flow closer to the core of the electrospray plume, where the droplet concentration is higher, will pick up charge while the rest will scape the device uncharged. In this regard, it would be interesting to include ion evaporation/emission from the electrospray droplets or even Coulomb fissions, since probably the presence of smaller charged entities, with larger mobilities and diffusivities, would help to increase the charging cross sections of sub-micron particles.

5. Conclusions

We have modeled a device for scavenging inertialess airborne microparticles by using an electrospray to charge and collect them. This device could be applied in testing gases for the presence of microparticles that might be of interest from a biological, safety or control applications, among others. It consists of a tube that ends on a plate with a concentric hole (extractor) located in front of a disk (collector). Coaxial with the tube is a second inner tube through which an electrospray is injected: the electrospray droplets move from the inner tube exit towards the extractor and the collector dragged by the electric field. The particles are injected through the annular gap between the tubes carried by a stream of gas that passes through the extractor hole. As they proceed through the extractor, they collide with the charged droplets, picking up one or several droplets and therefore becoming charged. The electric field now drag these charged particles towards the collector, where they are collected.

The mathematical model includes the steady-state continuity equations for the different species (droplets, neutral particles, etc.), the Poisson equation for the electric potential and the steady-state incompressible Navier–Stokes equations for the gas. The model includes the gas–particles interaction, as well as the *reactions* between the electrospray droplets and the particles in the limit where the electrospray droplet diameter is much smaller than the particle diameter, $d_e/d_p \ll 1$. An small artificial diffusivity is included to keep the numerical computations affordable.

The electrospray is assumed monodisperse in droplet size and also in charge per droplet. Also the particles are monodisperse.

The droplet–particle *reactions* reaction constants are written in terms of collision cross-sections that include inertial, diffusive and electrical effects. In the limit $d_e/d_p \ll 1$ the electrical effects, split into the external field effect and the image charge effect, dominate the collision process. The maximum number of electrospray droplets that a particle can collect, N, is calculated as part of the solution. Particle–particle interactions are not considered in view of the rather small particle-to-particle relative velocity.

For a fixed geometry and a fixed electrospray, the dimensionless problem depends on seven dimensionless parameters. The first six are gathered in (14) and are dimensionless measures of the voltages applied to the electrodes, V_0 and V_1, the total particle flux that enters the device, Φ_0, the particle laden gas velocity, v_{g_I}, the electrospray sheath velocity, v_{sh}, and the Reynolds number defined below (5'). The seventh parameter is the charge parameter $\hat{q}_e$ defined in (21), which depends on the particle diameter d_p. We have considered values of d_p from 0.5 up to 5 μm.

The limited numerical exploration of the parameter space that we have carried out reveals that the effect of the particles on the flow is crucial to achieve a high collection efficiency. Our simulations show that the momentum injected by the charged particles in the gas suffices to change the flow pattern computed in the absence of particles when the particle flux Φ_0 is higher than about 0.1. A gas recirculation region then appears around the corner of the extractor that helps focusing the particle-laden gas on the core of the electrospray plume. This increases the charging efficiency and thus the collection efficiency. The effect increases with the size of the particles because the particle–droplet collision cross-section roughly increases as d_p^2, and seems to be responsible for the rapid decline of the collection efficiency when the particle size falls below 2 μm. A possible limitation of this mechanism is the appearance of flow instability, which cannot be described with the steady-state model used here.

We have also run cases with very low particle fluxes, $\Phi_0 \sim 10^{-3}$. In this new situation, the inlet velocities of the carrier gas and the electrospray sheath, v_{g_I} and v_{sh}, must also be decreased to induce flow recirculation close to the extractor. When this is done, the collection efficiency increases for particles smaller than 2 μm, though again it drops to 57 % for $d_p = 0.5$ μm. More complete simulations are needed to fully characterize the system and ascertain the range of particle sized that can be efficiently captured with appropriate tuning of the operation parameters.

It would also be interesting to include ion evaporation/emission from electrospray droplets or even Coulomb fission. Possibly the presence of much smaller charged entities, with higher mobilities and diffusivities, would contribute to the charging kinetics.

Declaration of competing interest

The authors declare that they have no known competing financial interests or personal relationships that could have appeared to influence the work reported in this paper.

Data availability

No data was used for the research described in the article.

Acknowledgments

This work has been supported by the Ministerio de Ciencia e Innovación through grants PID-2020-115730GB-C21, PID-2020-115730GB-C22, and RED2018-102829-T.

Appendix A. Dimensionless reaction constants

To calculate the dimensionless reaction constants, $\hat{K}_i$, from the dimensional ones given in (17), K_i, one uses the characteristic value $K_c = v_c/(n_c L_1)$, so

$$\hat{K}_i = \frac{\sigma_i (z_e - z_i) E}{K_c} = \left[\frac{\pi \frac{d_p^2}{4} (z_e - z_i) E_c}{K_c} \right] \hat{y}^{*^2}(i, \tilde{q}_e) E,$$

and the dimensionless source terms are

$$\hat{w}_e = -\sum_{i=0}^{N-1} \hat{K}_i n_e n_i, \quad \hat{w}_0 = -\hat{K}_0 n_e n_0,$$

$$\hat{w}_i = \hat{K}_{i-1} n_e n_{i-1} - \hat{K}_i n_e n_i, \quad \text{for} \quad i = 1, 2, \ldots N-1,$$

$$\hat{w}_N = \hat{K}_{N-1} n_e n_{N-1},$$

where n_e, n_i are the dimensionless number concentration of the corresponding entity.

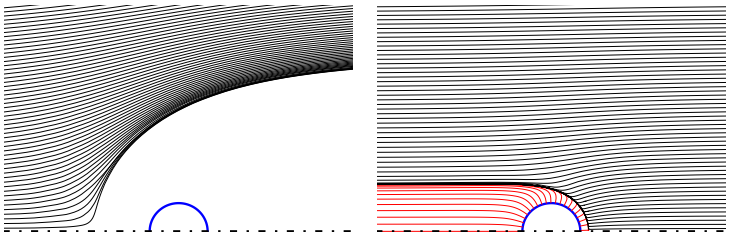

Fig. B.12. Pathlines followed from left to right by charged droplets in the presence of a pure conductive spherical particle and an external electric field for a charged particle with state of charge $i = 1$ and $q_e/E = 10$ (left) or $q_e/E = 1$ (right). The blue line represents the particle surface, red pathlines end up at the particle surface and black ones circumvents the particle thus avoiding collision. (For interpretation of the references to color in this figure legend, the reader is referred to the web version of this article.)

Appendix B. Droplet's pathlines around a particle

The pathlines followed by charged droplets around a particle, governed by (23), are depicted in Fig. B.12. Two representative cases are shown. On the left, the effective cross-section is zero, meaning that droplets never collide with the particle at those values of the local electric field and the electric charges of the droplet and the particle. On the right, we can observe a condition for which there exists a finite effective cross-section. Droplets falling within it, collide with the particle or they avoid collision elsewhere. No other pattern has been found.

Appendix C. Numerical procedure

The system of partial differential equations has been solved using the finite element method implemented by the software Comsol Multiphysics. The equations have been written in weak form in the general weak form PDE module, using linear elements for pressure p and quadratic ones for the rest of variables, such as the velocity field $\boldsymbol{v}$, the electric potential ϕ and the concentration fields of every species, n_e and n_i's. The use of this module requires the differential equations to be written in conservation form, as fulfilled,

$$\nabla \cdot \boldsymbol{j} = s\,, \tag{C.1}$$

where the generic flux vector $\boldsymbol{j}$ and the source term s depend on the variables and their gradients. The general Eq. (C.1) writes in weak form as $\int_{\mathcal{V}} (-\tilde{\varphi} s - \boldsymbol{j} \cdot \nabla\tilde{\varphi})\, \mathrm{d}\mathcal{V} + \int_{\partial\mathcal{V}} \tilde{\varphi}\boldsymbol{j} \cdot \boldsymbol{n}\, \mathrm{d}\Sigma = 0$, $\mathcal{V}$ being the domain and $\tilde{\varphi}$ a generic test function.

Additionally, a continuation method has been used to enhance the convergence of the numerical methods when solving the strongly coupled and nonlinear system of PDEs here considered. To do so, first the gas mass and momentum conservation (4), (5) together with the electric field (3) and the electrospray concentration (1) has been solved. Next, particles are added to the simulations considering (2), starting with neutral particles for $i = 0$, and once the previous step is converged the considered maximum state of charge of the particles is increased one by one until the desired value is achieved. Independence of the mesh has been checked and diffusion coefficients have been used for the sake of numerical stability while being small enough to avoid influencing the computed efficiency of the device.

Finally, the computation of the path of the droplets needed to characterize the collision cross-section have been carried out using the software Matlab and the built-in explicit solver of nonstiff differential equations implemented in the ode45 command, which is based on an explicit Runge–Kutta (4,5) formula, the Dormand-Prince pair.

References

Ahn, J. H., Yoon, J. U., Kim, K. Y., & Ahn, K. H. (2003). Performance of electrostatic precipitator using electrospray charging method. *Journal of Aerosol Research*, *18*, 98–102.

Bango, J. J., et al. (2021). A pandemic early warning system decision analysis concept utilizing a distributed network of air samplers via electrostatic air precipitation. *Applied Sciences*, *11*(11), 5308.

(2021). *COMSOL multiphysics v. 6.1*. Stockholm, Sweden: COMSOL AB, www.comsol.com.

Dunnett, S. (2013). Filtration mechanisms. In I. Colbeck, & M. Lazaridis (Eds.), *Aerosol science: technology and applications* (p. 2013). Wiley Online Library, http://dx.doi.org/10.1002/9781118682555.ch5.

Dziekan, M. (2012). *Electrospray collection of lunar dust*: *NASA tech. brief, LEW-18629-1*.

Fenn, J. B. (2004). *Electrospray air sampler*: *US2004/0023411 A1*.

Fernández de la Mora, J., & Loscertales, I. G. (1994). The current emitted by highly conducting taylor cones. *Journal of Fluid Mechanics*, *260*, 155–184.

Johnstone, H. F., & Roberts, M. H. (1949). Deposition of aerosol particles from moving gas streams. *Industrial and Engineering Chemistry*, *41*, 2417–2423.

Khalifehei, M., & Higuera, F. J. (2020). Neutralization of an electrospray by a corona discharge. *Journal of Aerosol Research*, *145*, Article 105547.

Kim, J.-H., Lee, H.-S., Kim, H.-H., & Ogata, A. (2010). Electrospray with electrostatic precipitator enhances fine particles collection efficiency. *Journal of Electrostatics*, *68*, 305–310.

Lear, C. W., Krieve, W. F., & Cohen, E. (1975). Carged droplet scrubbing for fine particle control. *Journal of the Air Pollution Control Association*, *25*, 184–189.

Loscertales, I. G., & Fernández de la Mora, J. (1995). Experiments on the kinetics of field evaporation of small ions from droplets. *The Journal of Chemical Physics*, *103*, 5041–5060.

Pilat, M. J. (1975). Collection of aerosol particles by electrostatic droplet spray scrubbers. *Journal of the Air Pollution Control Association*, *25*, 176–178.
Prem, A., & Pilat, M. J. (1978). Calculated particle collection efficiencies by single droplets considering inertial impaction. *Atmospheric Enviroment*, *12*, 1981–1990.
Stommel, Y. G., & Riebel, U. (2005). A corona-discharge-based aerosol neutralizer designed for use with the SMPS-system. *Journal of Electrostatics*, *63*, 917–921.
Tepper, G., & Kessick, R. (2008). A study of ionization and collection efficiencies in electrospray-based electrostatic precipitators. *Journal of Aerosol Research*, *39*, 609–617.
Tepper, G., Kessick, R., & Pestov, D. (2007). Electrospray-based, ozone-free air purification technology. *Journal of Applied Physics*, *102*, Article 113305.